Bias in Mean Vertical Wind Measured by VHF Radars: Significance of Radar Location Relative to Mountains

R. M. WORTHINGTON

Cooperative Institute for Research in Environmental Sciences, University of Colorado, Boulder, Colorado

A. MUSCHINSKI

Cooperative Institute for Research in Environmental Sciences, University of Colorado/NOAA/Environmental Technology Laboratory, Boulder, Colorado

B. B. BALSLEY

Cooperative Institute for Research in Environmental Sciences, University of Colorado, Boulder, Colorado

(Manuscript received 14 March 2000, in final form 14 July 2000)

ABSTRACT

Measurements by VHF wind-profiling radars worldwide have, for many years, shown long-term downward atmospheric motion in most of the troposphere. Various explanations have been proposed, some atmospheric and some caused by the radar measurement method. At many sites, except those in the Tropics, the authors suggest a new model, in which the long-term downward vertical wind ($\overline{W}$) is real and atmospheric, a consequence of radars being constructed on low ground near or within mountain ranges, so that they tend to view on average the same phase of mountain waves. A coincidence consisting of five factors—low-lying radar locations near mountains, the upwind slope of untrapped mountain wave phase lines with height, the inability of wind-profiling radars to measure both the lowest few kilometers of the troposphere and far into the stratosphere, decreasing tropospheric static stability with height, and increasing tropospheric wind speed with height—has led to downward $\overline{W}$ measurements in most of the troposphere. The new mountain wave model applies to all types of wind-profiling radars and lidars, and may account for unexplained $\overline{W}$ observations at many sites.

1. Introduction

VHF wind-profiling radars probably offer the best hope of measuring continuously the vertical wind, with good height and time resolutions. The vertical wind (W) or its long-term time average ($\overline{W}$), if it can be measured reliably, is of direct importance for numerical weather prediction (e.g., Van den Dool 1990), and efforts have been made to measure it using VHF and UHF radars, for many years and with only partial success. Although synoptic-scale vertical winds are only a few centimeters per second at most, they ought to be measurable by radar (Nastrom 1984; Nastrom et al. 1985), even, theoretically, in mountainous areas where mountain waves cause $|W| > 1$ m s^{-1}, provided the phase of the wave patterns above the radar is random over time (Nastrom et al. 1985).

Instead, VHF radars worldwide find a downward midtropospheric $\overline{W}$, which has been attributed to many possible causes, involving either real atmospheric motion or false effects arising from the radar measurement technique. Five possible models are:

1) Real vertical-wind circulation linked to the jet stream or jet streaks (Yoe and Rüster 1992; Takayabu et al. 2000; Rao et al. 2000; Faust 1962).
2) In the Tropics, real vertical winds linked to convection and radiative balance (Balsley et al. 1988; Gage et al. 1991, 1992; Huaman and Balsley 1996).
3) False measurement, caused by a correlation between gravity wave perturbations of stability and velocity, within the radar sampling volume and time (Nastrom and VanZandt 1994, 1996), and the effect of missing data in conditions of poor signal-to-noise ratio (SNR) (Hoppe and Fritts 1995).
4) False measurement, caused by tilted VHF-aspect-sensitive scatterers linked to Kelvin–Helmholtz instability (KHI) (Muschinski 1996), in regions of vertical shear of the horizontal wind, below and above the jet stream.

Corresponding author address: R. M. Worthington, CIRES, University of Colorado, Campus Box 216, Boulder, CO 80309-0216.
E-mail: worth@terra.colorado.edu

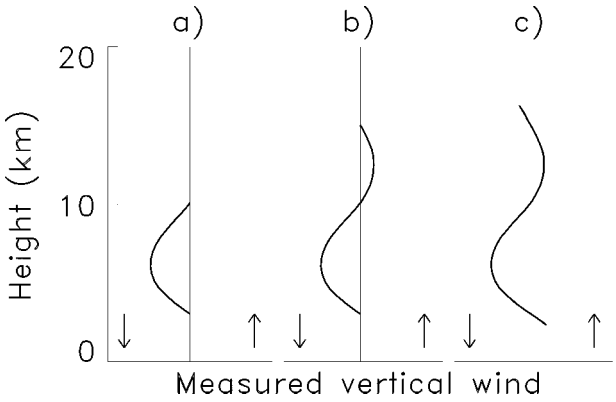

FIG. 1. Diagram of mean vertical-wind profiles reported and modeled in previous studies. In the simplest case, a, downward W is measured in the midtroposphere. However, extra reversals of sign, cases b and c, are often found. In all three cases, downward $\overline{W}$ is observed in the midtroposphere.

5) A real, residual mountain wave component, because the phase of mountain waves above radars is not completely random (Worthington 1999a).

This paper studies why the positions of mountain wave patterns above a radar might be nonrandom (model 5) in such a way as to give downward $\overline{W}$ in most of the troposphere. A new explanation for downward tropospheric $\overline{W}$ is based here on the tradition and/or necessity of building VHF radars on flat ground, low-lying relative to the surroundings, rather than on mountain slopes or high ground. Balsley and Carter (1989) already note the possibility of mountain waves having a ''preferred phase relationship relative to [a] region of balloon ascents, or to the antenna beam of a wind profiler.'' If wind-profiling radars and lidars, worldwide, are installed in similar locations relative to mountains, the resulting phase relation to mountain waves, and the effect on $\overline{W}$, might be similar.

The averaging timescale for $\overline{W}$ studied here, where VHF radar validation is the aim, is typically years—in fact as long as possible, since $\overline{W} \approx 0$ averaged over many years and worldwide is necessary, but not sufficient, before trusting point measurements of synoptic-scale $\overline{W}$ by radars. The timescales of interest in synoptic-scale $\overline{W}$ are whatever is required in numerical modeling studies, typically hours or days.

A first problem is to decide the exact $\overline{W}$ profile that must be explained. Figure 1a shows the most obvious feature is downward $\overline{W}$ in the midtroposphere, approximately 3–10 km, which can be explained by model 3 (Nastrom and VanZandt 1994), assuming that upward-propagating gravity waves predominate in the troposphere. However, $\overline{W}$ is also often found to reverse sign and be upward in the lower stratosphere (McAfee et al. 1989; Yoe and Rüster 1992; Nastrom and VanZandt 1994; Nastrom and Eaton 1995) as shown in Fig. 1b. In model 3 this would require a majority of gravity waves, in the lower stratosphere, propagating downward from a source somewhere higher than the radar can measure. Little observational evidence exists for this. Nevertheless, the $\overline{W}$ profile in Fig. 1b could still be explained by models 1, 2, 4, and 5, with a contribution from model 3 in the troposphere.

Muschinski (1996) shows that $\overline{W}$ as in Fig. 1b might result from KHI, model 4, causing tilting of VHF-aspect-sensitive scatterers (Fig. 2a) in regions of vertical shear of horizontal wind, above and below the jet wind maximum. These tilted scatterers pull the effective pointing angle of a vertical VHF radar beam slightly off vertical. Since the wind shear vector is often nearly parallel to the strong, sheared jet stream winds, but its direction, and therefore the alignment of KHI, reverse above and below the jet maximum (See Fig. 1 of Muschinski 1996), the vertical radar beam effectively points slightly upwind (below the jet wind maximum) or downwind (above the jet maximum). Therefore, a spurious downward $\overline{W}$ is seen below the jet maximum, and upward $\overline{W}$ is seen above. Evidence for this, using echo power imbalances between symmetric radar beams, is shown by Worthington and Thomas (1996b, 1997a). However, the precise magnitude of the KHI effect on

	a) Horizontal airflow containing tilted aspect-sensitive scatterers (e.g. from KHI) RADAR	b) Airflow and aspect-sensitive scatterers both tilted, as they pass through a mountain wave RADAR
Real vertical wind	zero	U sinδ
Vertical wind measured by VHF radar	non-zero, downward	< U sinδ

FIG. 2. Diagram showing the effect of tilted aspect-sensitive scattering layers on VHF vertical-beam wind measurements. (a) The airflow is horizontal and vertical wind W is zero, but the scatterers within it are tilted, causing VHF radar to measure falsely a nonzero, downward vertical wind (Muschinski 1996). (b) Both the airflow and scatterers are tilted, for instance, by a mountain wave (Worthington 1999a), and the magnitude of the W measurement is reduced slightly because the effective VHF vertical-beam direction is pulled slightly toward perpendicular to both the airflow and the scattering layers within it.

TABLE 1. Locations of VHF wind profilers worldwide.

	Latitude (°N)	Longitude (°E)	Range of land height in Fig. 10 according to GLOBE database (meters above sea level)
Aberystwyth, Wales	52.42	−4.00	0–1068
Andenes, Norway	69.30	16.01	0–1200
Arecibo, Puerto Rico	18.35	−66.75	0–1280
Biak, Indonesia	−1.18	136.12	0–1426
Birdlings Flat, New Zealand	−43.83	172.67	0–1784
Buckland Park, Australia	−34.63	138.48	0–633
Christmas Island, Kiribati	2.00	−157.42	0–6
Chung-Li, Taiwan	24.58	121.00	0–3772
Clermont-Ferrand, France	45.71	3.09	155–1756
CLOVAR, Canada	43.07	−81.34	174–518
Darwin, Australia	−12.43	130.95	0–283
Flatland, USA	40.05	−88.38	130–285
Gadanki, India	13.47	79.18	0–1322
Jicamarca, Perú	−11.95	−76.87	0–5536
Kennedy Space Center, USA	28.63	−80.70	0–85
Kiruna/ESRANGE, Sweden	67.88	21.10	141–1120
Kühlungsborn, Germany	54.12	11.77	0–149
La Ferte Vidame, France	48.62	0.88	0–399
Lannemezan, France	43.12	0.37	28–3276
Launceston, Australia	−41.54	147.20	0–1522
Lonate Pozzolo, Italy	45.34	8.43	0–4469
Machu Picchu, Antarctica	−62.09	−58.47	0–622
Mount Gambier, Australia	−37.75	140.79	0–310
MU, Japan	34.85	136.10	0–1773
Piura, Perú	−5.17	−80.64	0–3656
Platteville, USA	40.18	−104.73	1295–4233
Pohnpei, F.S. Micronesia	6.96	158.19	0–655
Poker Flat, USA	65.13	−147.46	97–1493
Resolute Bay, Canada	74.69	−94.81	0–376
SOUSY, Germany	51.66	10.49	0–1056
Saint Lary, France	42.82	0.28	21–3276
Sunset, USA	40.04	−105.45	1386–4334
Sydney, Australia	−33.93	151.17	0–1143
Toulon, France	43.12	5.92	0–2518
Toulouse, France	43.57	1.37	30–3246
Urbana, USA	40.15	−88.15	134–285
Ushuaia, Argentina	−54.08	−68.03	0–1464
Vandenburg, USA	34.77	−120.53	0–1980
Wakkanai, Japan	45.36	141.81	0–1451
White Sands, USA	32.40	−106.35	1080–3602

$\overline{W}$ remains unknown at present. Other configurations of airflow and tilted scatterers will have a variety of effects. For instance, for wind flow tilted from horizontal in a mountain wave, containing aspect-sensitive layers that are similarly tilted from horizontal (Gage 1986; Worthington 1999a), the real mountain wave W will be slightly reduced when measured by a vertical VHF radar beam, because the effective beam-pointing direction is pulled slightly toward perpendicular to both the airflow and the layers within it (Fig. 2b).

When measuring over a height range 1.7–21 km (Worthington 1999a, his Fig. 10, using the Aberystwyth VHF radar), it appears there are further reversals in the sign of $\overline{W}$, as shown in Fig. 1c. Figure 1c cannot be easily explained by any of models 1–4 but might be explained by mountain wave model 5. The height range of radar $\overline{W}$ measurements is often limited, for instance, Nastrom and Eaton (1995) show $\overline{W}$ measurements above 7 km only, because of technical problems at lower heights, and few studies show data below 3 km. This makes it difficult to distinguish between the situations in Figs. 1a–c. However, at many sites, and not only Aberystwyth, it might actually be Fig. 1c, not just Fig. 1a or b, that must be explained.

Considering model 5, many of the VHF wind-profiling radars built so far (e.g., Fig. 10 and Table 1, later) are located not just in or near mountains but in valleys, plains, or relatively low-lying ground in mountainous areas. VHF radars usually need to be built on a flat horizontal area of ground, typically ~100 m × 100 m, so sloping valley sides are unsuitable. Sites in the base of valleys, or on low plains near mountains, have traditionally been used rather than flat mountaintop areas—possibly for shelter, and for convenience since most roads and settlements are sited in valleys. [Two very rare exceptions of mountaintop acoustic radars, although with no $\overline{W}$ measurements, are described by Asimakopoulos et al. (1980) and Gardiner and Hill (1986)]. Also,

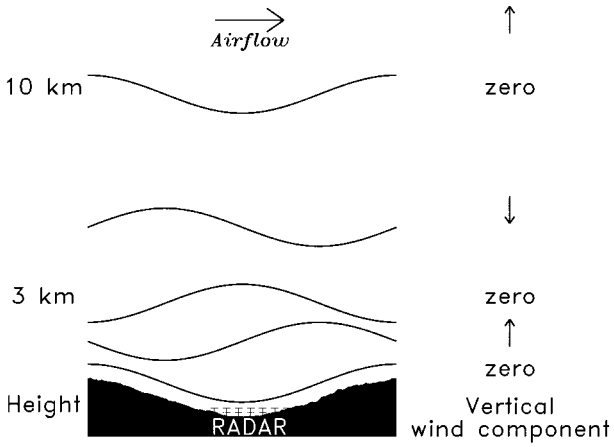

FIG. 3. Vertical cross section of a typical radar location in the base of a valley, showing the phase variations of the streamlines of untrapped mountain waves. Lines of constant phase move upwind with increasing height. The resulting phase relation between radar location and mountain waves gives mostly nonzero long-term mean vertical wind $\overline{W}$, with downward $\overline{W}$ in most of the troposphere. The same $\overline{W}$ profile would result if wind flow was from right to left, instead of left to right. For many radars including Aberystwyth, the land height on one side is less than the other, but the same qualitative $\overline{W}$ profile should result. Height variations of the streamlines are exaggerated for clarity.

wind profilers are more frequently being installed near airports, where the requirement for large, flat horizontal areas, often relatively low lying, is even greater. However, as outlined in Fig. 3, this introduces a risk that mountain waves are at least slightly phase-locked to the underlying terrain, and so to the radar location.

For hydrostatic mountain waves, the vertical wavelength is given by

$$\lambda_z = \frac{2\pi}{m} = \frac{2\pi U}{N} \tag{1}$$

(e.g., Hines 1989), where m, N, and U are vertical wavenumber, Brunt–Väisälä frequency, and wind speed, respectively. Assuming W is zero near the ground surface (Fig. 3), model 5 predicts a relatively small region of upward W in the lower troposphere and a deeper region of downward W above in most of the troposphere, in the height range many wind-profiling radars measure. The height region of downward W is deeper, because U typically increases and N decreases with increasing height in the troposphere, both these factors causing an increase of λ_z for mountain waves. Further reversals in sign of $\overline{W}$ with increasing height would be expected. Therefore, the predicted $\overline{W}$ profile in Fig. 3 is qualitatively the same as Fig. 1c and Worthington (1999a, Fig. 10).

This paper is organized as follows. In section 2 we examine $\overline{W}$ profiles from VHF radars at both a tropical and midlatitude site. In section 3a mountain wave model 5 is tested with a case study, and in section 3b with 10 years of data. Since model 5 appears to work at the Aberystwyth radar, in section 3c its validity is investigated for radars worldwide, including in section 3d the limiting case of Flatland, where topographic effects are claimed to be negligible. Mountain waves rarely remain steady as in Fig. 3, so the variations of phase between the mountain waves and mountains, and the effect on $\overline{W}$, are studied in section 3e using satellite images. Section 3f reviews some further observations in terms of mountain waves.

2. Mean vertical-wind profiles observed at two latitudes

a. The Tropics: Piura, Perú

Studies using the National Oceanic and Atmospheric Administration (NOAA) Pacific profiler network show slight downward $\overline{W}$ in the tropical troposphere, measured by vertical radar beam during mostly clear conditions, which appears to agree with theory (model 2, Balsley et al. 1988; Gage et al. 1991). Considering the other models 1, 3, 4, and 5, tropical sites such as Piura and Christmas Island (Kiritimati), are relatively far from jet streams (model 1), and the vertical shear of horizontal wind (model 4), is usually more variable than simply reversing sign between troposphere and stratosphere (Huaman and Balsley 1996). Although there is mountain wave activity (model 5) in the Tropics (Balsley and Carter 1989), similar $\overline{W}$ results are seen both at Piura near the Andes Mountains (Huaman and Balsley 1996) and at Christmas Island (Gage et al. 1991), which is isolated and flat, suggesting that stationary mountain waves are not a dominant factor on $\overline{W}$ at Piura [although nonstationary mountain waves are seen at Piura (Liziola and Balsley 1998), and Christmas Island may act as a convective ''heat island'' disturbing the airflow, so a slight doubt remains]. Strong convection in the boundary layer and lower troposphere at Piura may generate upward-propagating gravity waves consistent with apparent downward tropospheric $\overline{W}$ in model 3; however, upward $\overline{W}$ is often measured in the tropical lower stratosphere, inconsistent with model 3. Also, the variance of W, a key parameter in model 3, is found by Huaman and Balsley (1996) to be sufficiently small in the Tropics that this model is not important. Therefore, models 1, 3, 4, and 5 may all be inadequate to explain $\overline{W}$ profiles from tropical wind profilers.

Figure 4 shows $\overline{W}$ from the radar at Piura (5.17°S, 80.64°W), Perú. Its operating frequency is 49.9 MHz, one-way half-power full beamwidth 3.4°, height resolution 1000 m, and peak transmitted power ~30 kW. Vertical beam-pointing precision was checked by Huaman and Balsley (1996) using array phasing measurements, so that the error in transmitted vertical-beam direction should be negligible. All five-beam data available at present, almost continuous from November 1994 to August 1997, are used. Here $\overline{W}$ can be measured by

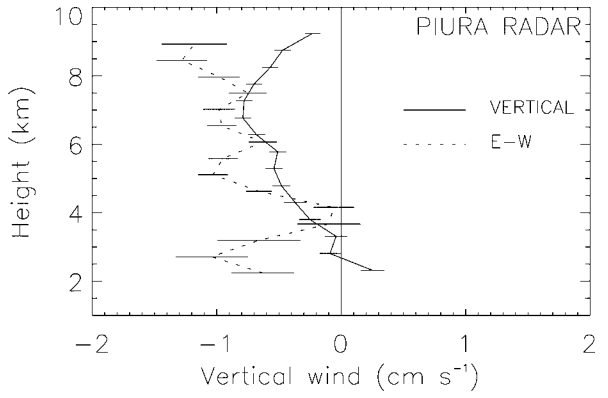

FIG. 4. Profiles of mean vertical wind $\overline{W}$ measured by the VHF radar at Piura, Perú, during Nov 1994–Aug 1997. Both the vertical beam (solid line) and a symmetric pair of beams 15° off-vertical in the east–west azimuth (dotted line) are used. The downward $\overline{W}$ of 0–1 cm s^{-1}, measured by both vertical and east–west beam combinations, agrees with earlier vertical-beam results from sites in the NOAA Pacific profiler network. Standard errors on the mean are plotted.

both the vertical beam, and symmetric pairs of beams 15° off-vertical, for instance,

$$W_{15^\circ} \approx \frac{v_n + v_s}{2\cos 15^\circ} \approx \frac{v_e + v_w}{2\cos 15^\circ} \approx \frac{v_n + v_s + v_e + v_w}{4\cos 15^\circ}, \quad (2)$$

where v_n, v_s and v_e, v_w are line-of-sight velocities in north–south and east–west symmetric beam pairs. Only data from the east–west pair of beams are used here, because of problems with the north beam. The height range of highest SNR, in the troposphere, is shown. The overall 0–1 cm s^{-1} downward $\overline{W}$ in Fig. 4, measured by both beam combinations, is in reasonable agreement with previous vertical-beam results from both the Piura and Christmas Island radars (Huaman and Balsley 1996; Gage et al. 1991). Since it appears that the sign and rough magnitude of radar $\overline{W}$ measurements in the Tropics may be real (model 2, Gage et al. 1991), we concentrate now on the much larger and poorly explained $\overline{W}$ measured at midlatitudes.

b. Midlatitudes: Aberystwyth, Wales

Ten years of five-beam data from the Aberystwyth meso-strato-troposphere (MST) radar, located 52.42°N, 4.00°W (Slater et al. 1992) are available, and are used next to investigate $\overline{W}$ profiles at midlatitudes. The VHF radar operating frequency is 46.5 MHz, one-way half-power full beamwidth 3°, height resolution typically 300 m, and peak transmitted power 160 kW. For all references to NW–SE and NE–SW beam azimuths, the exact values are N64°W–S64°E and N26°E–S26°W instead of N45°W–S45°E and N45°E–S45°W. The exact values are used in all calculations of wind components and directions.

The $\overline{W}$ measurements for June 1990–December 1997 by the Aberystwyth radar, over a large height range and using various radar-beam combinations, are shown by Worthington (1999a, Fig. 10). Figure 5 uses data from June 1990 to December 1999, with mean vertical, zonal, and meridional winds; wind direction; temperature; Brunt–Väisälä frequency; vertical-beam echo power; and number of data points, also using radiosonde data from the U.K. Meteorological Office station at Aberporth (52.13°N, 4.57°W). Radiosonde launches switched

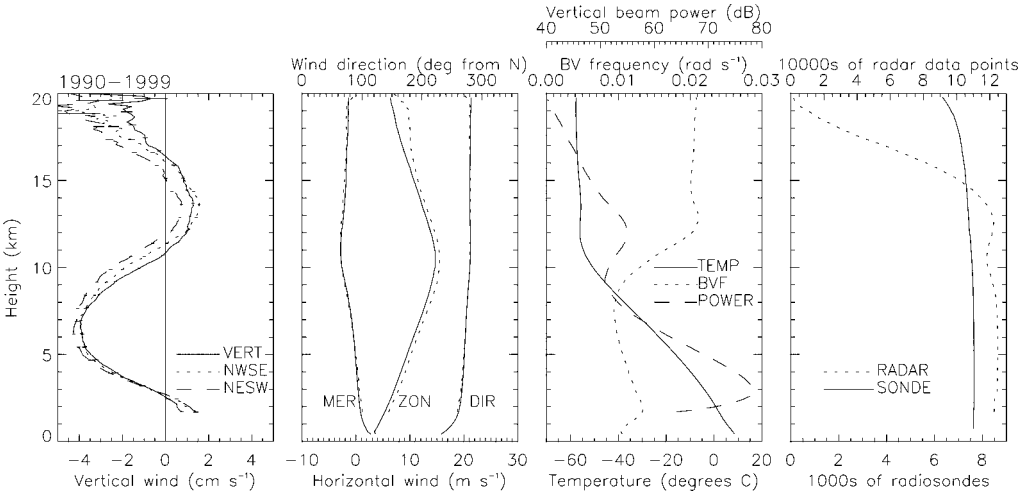

FIG. 5. Long-term mean profiles, Jun 1990–Dec 1999, of: vertical wind measured by a vertical radar beam, and by NW 6°–SE 6° and NE 6°–SW 6° symmetric beam pairs; average zonal and meridional wind profiles and direction, measured by radar (dashed lines) and radiosondes (solid lines); temperature, Brunt–Väisälä frequency and vertical-beam radar echo power; number of radar and radiosonde data points. Each of the many thousand radar data points is typically a 12-min average. Standard errors on mean $\overline{W}$ are plotted but negligible. Wind direction is from where the wind blows, measured clockwise from north, and upward W is defined as positive throughout the paper. Radar data are from the Aberystwyth MST radar, and radiosonde data from Aberporth.

from approximately daily to 6-hourly in April 1996, and the radar switched to almost continuous operation with at least five beams in October 1997, so there is an increasing amount of data in recent years.

Figure 5 shows that the $\overline{W}$ profile and its reversals with height are similar to Fig. 1c, rather than the simpler situations of Figs. 1a,b. The $\overline{W}$ reversal height near 10–11 km is very close to both the tropopause and the jet stream wind maximum, and it is unclear which, if either, is most relevant to the $\overline{W}$ profile. The $\overline{W}$ for individual years (not plotted) shows substantial interannual variation, although the overall shape remains similar to Fig. 1c. Above 17 km, where $\overline{W}$ becomes negative, the amount of data is decreasing (Hoppe and Fritts 1995); nevertheless, the three different beam combinations for measuring $\overline{W}$ all show downward motion, and varying the SNR cutoff changes details of the profiles, but has no significant effect on the sign of $\overline{W}$.

The sign reversal of $\overline{W}$ below 3 km in Fig. 5 is observed in conditions of highest SNR, with good agreement between beam combinations. This agreement is also shown in Worthington (1999a, Fig. 10) and a later case study, section 3a. Below 3 km, radar echo power is reduced on account of receiver overload, which might in theory affect the $\overline{W}$ measurements. However, as shown later in a case study, the region of upward W below 3 km sometimes moves up into the midtroposphere where the measurements are most reliable, as the phase of mountain waves shifts above the radar, and in dead-calm conditions W at all heights is very close to zero. The upward $\overline{W}$ below 3 km is of opposite sign to the expected effect of echoes from falling rain, and ground clutter would pull $\overline{W}$ toward zero rather than positive. Individual Doppler spectra appear qualitatively normal, there is relatively little VHF interference at the remote radar site, and the vertical and horizontal winds below 3 km height are accepted and used by the U.K. Meteorological Office. Therefore, the complete $\overline{W}$ profile as shown in Figs. 1c and 5 appears reliable, at least for the Aberystwyth radar, but it is consistent with model 5 only.

3. New mountain wave model for mean vertical wind, $\overline{W}$

a. Case study of 20 February 1999

A case study from 20 February 1999 is presented in Fig. 6, using data from the Aberystwyth radar. Here W in Figs. 6a–c shows bands of upward and downward vertical motion, similar to Yoe and Rüster (1992, Figs. 1, 2a,b, 3). Height–time plots of W often have this appearance when the jet stream is near the Aberystwyth radar, and another example is shown by Worthington (1999a, Fig. 7a). In general, vertical motion is downward in most of the troposphere, reverses sign near the tropopause and/or jet stream wind maximum, and is upward in the lower stratosphere. In this case study, however, some areas of evidence suggest that W is caused by mountain waves and not related directly to the jet stream.

1) Upward W is seen below ~3 km, and downward W above ~14 km, most clearly between 4 and 8 h. This matches Fig. 1c, and not Figs. 1a or 1b, which is consistent with mountain waves but not a simple jet stream W circulation.
2) At times, the W pattern in Figs. 6a–c changes and is briefly upward at all heights (13–14 h), or downward at all heights (16–17 h). These sudden changes in the sign of W, over a large height range, are easily possible for unsteady mountain waves (Worthington and Thomas 1998). Caccia et al. (1997a) state that W temporarily showing a ''wrong'' phase relation to the mountain, upward W in the lowest radar height gates above a mountain peak, may be incompatible with mountain waves. However, only a slight temporary variation of phase and vertical structure in the unsteady wave pattern above the radar is needed, for a few hours or less, then settling back to its usual state.
3) The vertical wavelength of W increases after about 13 h, so that the height of W reversal near 8 km moves up to 11 km. No clear corresponding change in tropopause height (Fig. 6d) or height of jet stream wind maximum (Fig. 6e) is seen, and the change in W appears unconnected with either. However, the jet stream horizontal wind above the radar (Fig. 6e) strengthens during the day, so the vertical wavelength of mountain waves would be expected to increase [Eq. (1)], and this is observed in Figs. 6a–c. Profiles are shown later in Fig. 7.

All three of these effects are also seen in Worthington (1999a, Fig. 7a). There are some further interesting features in Fig. 6, although not definite evidence for mountain waves.

1) Figure 6l shows an imbalance between NW and SE echo powers below 4 km and, in Fig. 6k, some smaller echo power imbalances of opposite sign between NE and SW beams. At first glance, these might appear to be radar problems; however, they match the W variations in Figs. 6a–c, in a region of tropospheric aspect sensitivity (Fig. 6j). Worthington (1999a,b) shows examples of mountain waves tilting VHF-aspect-sensitive scattering layers, causing echo power imbalances between symmetric pairs of beams; this effect can be used to calculate the alignment of mountain wave patterns. Similar early measurements, but using 0° and 7° radar beams, are described by Green and Gage (1980). They found that echo power in a beam 7° off-vertical was sometimes greater than in the vertical beam, implying scatterers tilted by more than 3.5° from horizontal in a very mountainous area. A mountain-wave pattern with horizontal wavevector aligned near NW–SE could explain the power imbalances below 4 km in Fig. 6k,l; from the method

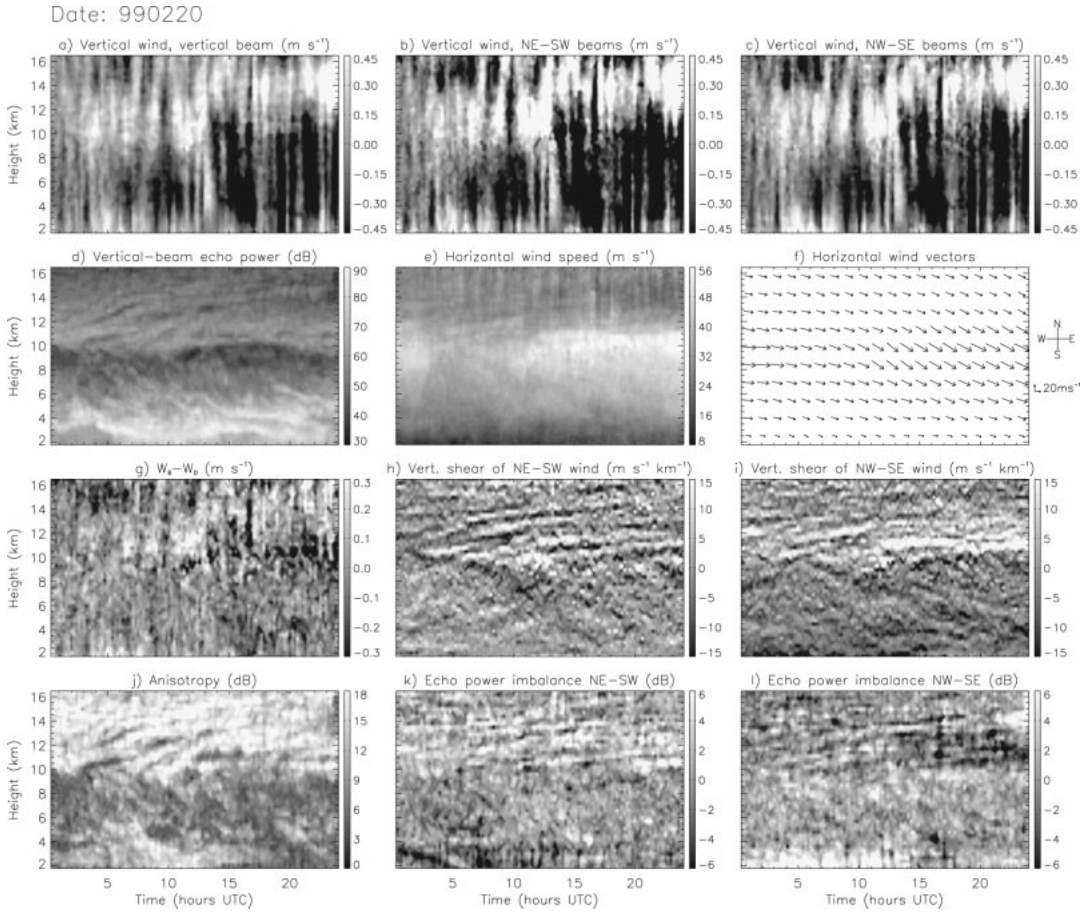

FIG. 6. Height–time plots for 20 Feb 1999 using the Aberystwyth VHF radar, showing (a), (b), (c) mountain waves in the troposphere and lower stratosphere and (e), (f) a strong jet stream. Plots (a), (b), (c) show vertical wind *W* measured by a vertical beam, and by NE 6°–SW 6° and NW 6°–SE 6° symmetric beam pairs, respectively. (g) The difference between vertical-beam and 6° beam estimates of *W* is close to zero in the troposphere, but the vertical beam underreads the magnitude of *W* in (d), (j) aspect sensitive conditions above ~9 km, in the stratosphere. (j) Anisotropy is the difference between vertical and average 6° beam echo powers. Other plots are discussed in the text.

of Worthington (1999a), the average alignment of the horizontal mountain wave vector on this day is toward N84°W. Some echo-power imbalances are also seen above 10 km (Worthington and Thomas 1997a) that match with layers of wind shear that are moved upward as the jet stream approaches.

2) The difference between *W* measured by the vertical beam and by averaging line-of-sight velocities in all four 6° beams (Fig. 6g), is not always zero and has features above 10 km that appear to be correlated with *W* in Figs. 6a–c. In aspect sensitive conditions above 10 km, in the stratosphere, the vertical beam is underreading slightly the magnitude of mountain wave *W*, relative to the average of Figs. 6b,c. This could be explained if the effective vertical-beam direction is pulled slightly toward perpendicular to the tilted layers and airflow, as in Fig. 2b (e.g., Röttger et al. 1990; Van Baelen et al. 1991; Palmer et al. 1991), whereas the velocities measured in 6° beams are slightly less affected by aspect sensitivity. Larsen et al. (1991) also find that estimates of *W* using VHF vertical and off-vertical beams agree best when aspect sensitivity is weak. Some interesting variations in horizontal wind speed above 12 km (Fig. 6e) are discussed later in section 3f.

Figure 7 shows two wind profiles by radar, radiosondes, and the National Centers for Environmental Prediction (NCEP) Global Data Assimilation System (GDAS) model, at 0600 and 1800 UTC on 20 February 1999, close to Aberystwyth. The four data points nearest to the radar are averaged together. All three methods of measuring zonal and meridional wind agree well, showing that the radar and GDAS model are self-consistent.

The *W* measured by various combinations of radar beams (two vertical-beam measurements in each cycle, a NW 6°–SE 6° symmetric beam pair, and a NE 6°–SW 6° symmetric beam pair) are also self-consistent in Fig. 7. However, the model/radar comparison for *W* is extremely poor. At 0600 UTC, GDAS-model *W* shows

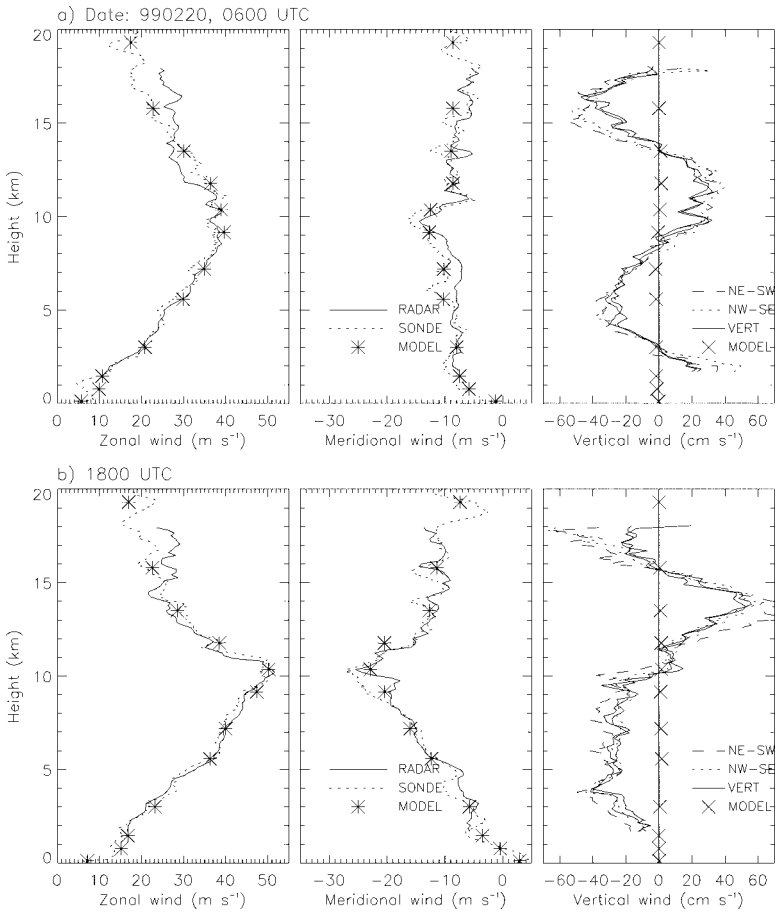

FIG. 7. Profiles of zonal, meridional, and vertical wind components measured at (a) 0600 UTC and (b) 1800 UTC on 20 Feb 1999 by three methods: the Aberystwyth radar, radiosondes launched from Aberporth, and the GDAS numerical model. Radar winds are 2-h averages centered on the times of the other measurements. The zonal and meridional winds show excellent agreement between measurements and GDAS model, but the wavelike structure in the radar-measured vertical wind W is not found in the GDAS model, consistent with local mountain wave activity that is not resolved in the model.

descent below the jet maximum and ascent above, but only of ± 2 cm s^{-1}, whereas the radar W is in excess of ± 20 cm s^{-1}. Fukao et al. (1991) similarly find that synoptic W in conditions of strong jet stream is often much smaller than radar W, and commonly of different sign. One possibility (Fukao et al. 1991) is that radar W may be showing small-scale atmospheric features, persisting above the radar for long times, that are difficult to distinguish from real synoptic $\overline{W}$; wind-profiling radars give only limited information about the synoptic-scale variability of the wind vector. In the present case study, it appears that these persistent features of small horizontal scale above the radar, causing nonzero $\overline{W}$, are mountain waves as shown in Fig. 3.

b. Simple model of hydrostatic mountain waves

We examine now in detail if long-term $\overline{W}$ measurements at Aberystwyth, as shown earlier in Fig. 5, and which appear similar to the mountain wave case study in Fig. 7, are also consistent with mountain waves. Figure 8 uses the entire five-beam output of the Aberystwyth radar for 10 yr, June 1990–December 1999, with $\overline{W}$ calculated from all four 6° beams [see Eq. (2)], although vertical-beam results are almost identical.

Diurnal variations of $\overline{W}$ have been reported in the Tropics (e.g., Gage et al. 1992). However, after sorting 10 yr of W profiles according to time of day, and then averaging, Fig. 8a shows little obvious diurnal effect on $\overline{W}$ at this midlatitude location. A relation between the $\overline{W}$ profile and jet stream strength is reported by Fukao et al. (1991), so the two right-hand columns of Fig. 8 are sorted according to the mean horizontal wind speed at 9–12 km height, which is the approximate height of maximum jet wind at this latitude. The reported relation of $\overline{W}$ to jet wind speed in previous studies is the reason that this method of data sorting is used here. Sorting

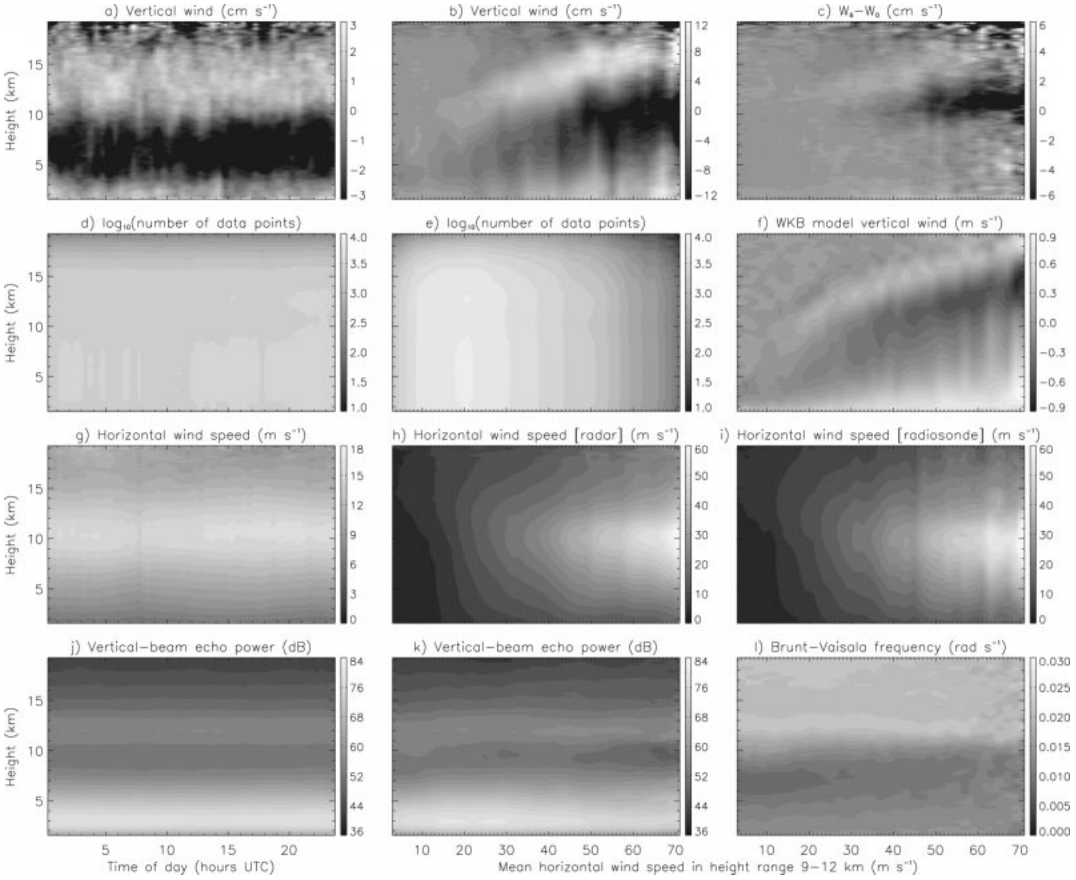

FIG. 8. Diurnal variation of (a) vertical wind $\overline{W}$, (d) number of data points, (g) horizontal wind speed, and (j) vertical-beam echo power to monitor the tropopause height and structure. The $\overline{W}$ in (a) shows little obvious diurnal change. Other plots: same as a, d, g, j, but as a function of jet stream strength (mean horizontal wind speed between 9- and 12-km height) for comparison with earlier studies. The vertical wavelength of $\overline{W}$ oscillation in (b) increases as the horizontal wind speed increases, yet (h) the height of jet maximum and (k) tropopause shown by vertical-beam echo power remain near 10 km. (c) The difference between $\overline{W}$ measured by vertical and by the 6° beams; the difference is small in the troposphere, but the vertical beam underreads in more aspect-sensitive conditions in the stratosphere. (f) A simple WKB model for $\overline{W}$, using (i), (l) wind speed and Brunt–Väisälä frequency measured by radiosondes. The vertical wavelength and phase of $\overline{W}$ predicted by this mountain wave model, as a function of jet wind speed, agree well with observations in (b). All available five-beam Aberystwyth data for Jun 1990–Dec 1999, several hundred days, are used.

the data according to maximum horizontal wind speed at any height also gives similar results.

The height of maximum horizontal wind speed (Fig. 8h) and tropopause shown by radar echo power (Fig. 8k) remain close to 10 km, independent of the speed of the jet stream wind. However, the height of $\overline{W}$ reversal (Fig. 8b) moves up by several kilometers as a function of increasing jet wind speed, from approximately 7 to 12 km. The $\overline{W}$ reversal height moves from below to above the average height of both the tropopause and maximum jet wind speed, with apparently little relation to either, similar to W in Figs. 6a–c. Although mountain wave reflection at the tropopause has been reported in case studies (Worthington and Thomas 1997b), it appears to be much less important in the long term. Upward $\overline{W}$ is seen, as before, below 3 km. An increase in λ_z of mountain waves would be expected in increasing horizontal winds [Eq. (1)], so that Fig. 8b is qualitatively consistent with $\overline{W}$ caused by mountain waves. Note that as the jet wind speed increases from, for instance, 35 to 70 m s^{-1}, the increase in λ_z is less than double, because the region of upward $\overline{W}$ near 8–18 km in Fig. 8b is being moved up into the stratosphere, where the approximate doubling of Brunt–Väisälä frequency, compared to the troposphere, acts to reduce λ_z.

To test quantitatively whether λ_z and phase of $\overline{W}$ in Fig. 8b are consistent with mountain waves, $\overline{W}$ predicted by a simple Wentzel Kramer Brillouin (WKB) model (e.g., Gill 1982), again sorted as a function of 9–12-km jet wind speed, is shown in Fig. 8f. Predicted W at height h is given by

$$W(h) \propto \sin\left(\int_0^h N(z)/U(z)\, dz\right), \qquad (3)$$

where z is height, and assuming $W(z) = 0$ at $z = 0$ as

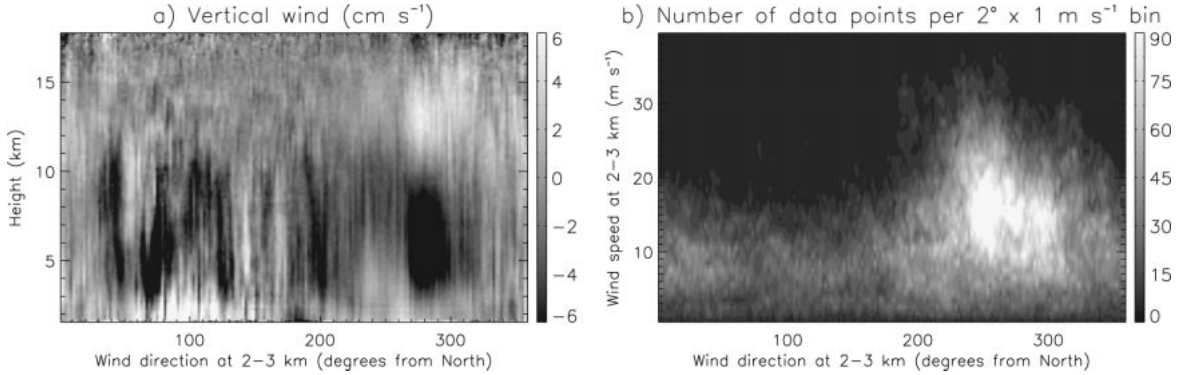

FIG. 9. Dependence of long-term mean vertical wind $\overline{W}$ on low-level horizontal wind direction at Aberystwyth, Jun 1990–Dec 1999. Wind direction is from where the wind blows, measured clockwise from north. Here $\overline{W}$ profiles as in Fig. 1c are not found for all wind directions, but the results are heavily weighted according to the prevailing westerly winds.

in Fig. 3, because the Aberystwyth radar is on low ground. The WKB model is applied to individual radiosonde profiles, not the average wind and stability data in Figs. 8i,l. The model W amplitude for each profile is set to 1 m s^{-1}. Data as low as 0.2-km height are supplied by more than 7000 radiosondes launched nearby at Aberporth during 1990–99 (Figs. 8i,l), although the region below 1.5 km is not plotted in order that the height range in all parts of Fig. 8 is the same. The radar and radiosonde horizontal winds in Figs. 8h and Fig. 8i agree, and the tropopause shown by increased Brunt–Väisälä frequency (Fig. 8l) and radar echo power (Fig. 8k) also agree. Note that the mean horizontal-wind profiles in Fig. 5 cannot be used to calculate λ_z, since the average speed is reduced by the inclusion of many calm days with no mountain waves.

For all wind speeds, including the range 40–70 m s^{-1} [approximately the regime considered by Fukao et al. (1991) and Yoe and Rüster (1992)], the WKB mountain wave model in Fig. 8f is very similar, in terms of vertical wavelength and phase, to measured $\overline{W}$ in Fig. 8b. Some phase disagreement in Fig. 8f might be caused by neglected effects on wave structure, such as high humidity and heavy rain that often accompany low-pressure weather systems with strong jet stream winds at Aberystwyth, and also changes in the effective horizontal phase relation between radar site and mountains (Fig. 3) as a function of wind speed. Overall, Fig. 8b appears consistent with hydrostatic mountain waves, presumably generated by the large-scale ''envelope'' of the Welsh mountains and not the detailed hills and valleys of horizontal scale only a few kilometers. Wallington (1961) shows measurements from five flights by instrumented aircraft above Aberystwyth and the Welsh mountains in 1957–58, in conditions of strongest westerly jet stream winds. The potential temperature crosssections showed wavelike structure with horizontal wavelengths similar to the overall width of the mountains, ~100 km. However, whatever the horizontal scale of hills and valleys that are generating the waves (if, e.g., the topography could be bandpass filtered), the Aberystwyth radar, at only 40 m above sea level, is generally on the lowest ground. Considering horizontal scales of only a few kilometers, the radar is in the base of the valley of Afon Peithyll, among small hills near the coast; considering scales of hundreds of kilometers, it is on low ground relative to the main Welsh mountains. Whether the horizontal scale in Fig. 3 represents anything from, for instance, 1–100 km, the radar has the right phase relation to the mountains, located on the lowest ground, for the mountain wave $\overline{W}$ model in Fig. 3.

For completeness, Fig. 9 shows the dependence of long-term $\overline{W}$ on low-level wind direction, using all data from June 1990 to December 1999 at Aberystwyth. As in Fig. 8, $\overline{W}$ is calculated from an average of all four 6° beams. A similar figure, but looking at the mean of $|W|$ instead of W, is shown by Worthington and Thomas (1996a, Fig. 11). For low-level winds of 90° and 270°, when the radar is simply downwind or upwind of the center of the Welsh mountains, $\overline{W}$ is upward in the lowest troposphere and downward in the mid/upper troposphere, as in Fig. 1c and 3. When the wind is more nearly parallel to the coast, flowing across the complex peninsulas and hills of the west coastline of Wales, the simple model in Fig. 3 breaks down as expected, and the $\overline{W}$ profiles in Fig. 9a are more complicated. Bishop (1968) also reports that mountain waves above Wales are more complex and variable for low-level wind directions outside the range 240°–300°. The results are heavily weighted by the prevailing westerly winds, so that overall $\overline{W}$ in Fig. 5 remains similar to Fig. 1c.

c. *Locations of wind profilers worldwide relative to mountains*

To investigate whether VHF wind-profiling radars worldwide might suffer similarly because of their location on low ground, Fig. 10 and Table 1 show the topography in 2° lat × 2° long areas centered on the sites of 40 existing or former radars. Unfortunately, the latitudes and longitudes are not entirely accurate to 2 decimal places, because of differing values in the pub-

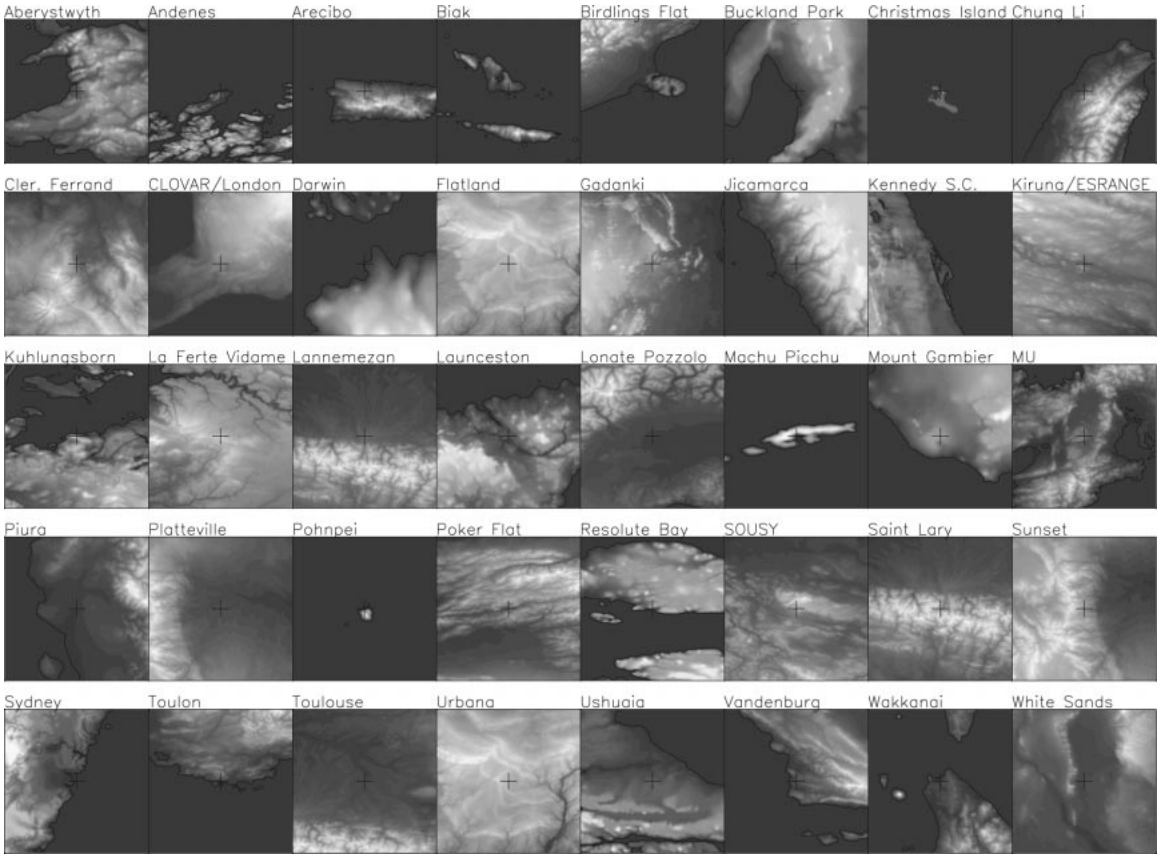

FIG. 10. Maps of the terrain height surrounding VHF wind-profiling radars across the world. Each map covers 2° long × 2° lat, centered on the radar location, which is marked by a cross. The range of shading is stretched to span the whole range of land heights in each 2° × 2° area; the range of land heights and the latitude and longitude of radars are listed in Table 1. Highest ground is lightest, and the coastline is drawn where applicable. Most radars are on low ground in otherwise mountainous areas, giving a possible bias in mean vertical wind $\overline{W}$, because of a tendency to be situated under the same phase of mountain wave patterns.

lished literature. The range of shading in each plot of Fig. 10 is adjusted to span the range of land heights within each 2° × 2° square, as listed in Table 1. Zero meters indicates sea level.

Every one of the radars, except Christmas Island, is located near hills or mountains, and most are on relatively low ground, consistent with model 5. A few possible exceptions, located on relatively high ground, are, for example, La Ferte Vidame, Saint Lary, and Mount Gambier. The $\overline{W}$ profiles from Saint Lary, part of the Pyrenean Experiment (PYREX) campaign (Bougeault et al. 1997), were calculated for the present study, but are not shown because of disagreements when using different pulse widths. Also, although only a few kilometers from the crest of the Pyrenées mountains, the Saint Lary radar was actually in a deep valley (Caccia et al. 1997a). More $\overline{W}$ profiles from many different sites would be very interesting, using both vertical and symmetric pairs of off-vertical beams if possible, and taken over several years, because Aberystwyth data show interannual variations in $\overline{W}$.

d. Topography of the Flatland radar site

Investigations of $\overline{W}$ at the Flatland Atmospheric Observatory describe the local topography as extremely flat (Nastrom and VanZandt 1994), with no topographic effects. Although there are locations with variations of terrain height less than 10 m over horizontal distances of hundreds of kilometers, for instance, areas of Florida, this is not the case at Flatland. Figure 10 and detailed topographic maps (U.S. Geological Survey 1957a,b) show the Flatland and Urbana radars (40.05°N, 88.38°W and 40.15°, 88.15°W, respectively; Warnock et al. 1994) are surrounded by gentle hills, including the range of low hills named Yankee Ridge, 50 m higher than the surroundings, at less than 10-km distance. Also, the city of Champaign–Urbana is sited on top of Yankee Ridge, close to and in between the Flatland and Urbana radar sites, which might, given typical heights of buildings, effectively increase the ridge height further by a few tens of meters. Hills of only 100 m are capable of generating some mountain waves (e.g., Lee and Neumark

1952; Bradbury 1965; Hensman 1971; Gedzelman 1977; VanValin et al. 1982; Lenschow et al. 1988; Prichard et al. 1995). Lee and Neumark (1952) describe glider flights in upward W greater than 1.5 m s^{-1} at a height of 0.7 km, downwind of a 75-m-high hill (51.87°N, 0.54°W) near Dunstable, England, in nonconvective conditions. Although W measured at the Flatland site is known to be dominated by nonorographic effects (Nastrom et al. 1990), this does not exclude faint mountain wave activity. Although perhaps a coincidence, and using only a five-day average, Warnock et al. (1994) report that $\overline{W}$ offsets at Flatland and Urbana were of opposite signs, -5 cm s^{-1} and $+2$ cm s^{-1}, respectively. The Flatland radar is on the lowest ground in the region, upwind of Yankee Ridge for prevailing westerly winds, whereas the Urbana radar is immediately to the lee of both the ridge and Champaign–Urbana city. Therefore, mountain wave model 5 would predict different $\overline{W}$ profiles at the two sites. However, it seems no long-term $\overline{W}$ measurements from Urbana are published, so this interpretation remains uncertain.

Although Caccia et al. (1997a) suggest that $|W| < 0.4$ m s^{-1} above the Pyrenées mountains cannot be mountain waves, smaller W perturbations above the Welsh mountains (Worthington and Thomas 1996a; Worthington 1998) do appear to be mountain waves. Maybe, extrapolating to lower topography (Caccia et al. 1997b), the 50-m hills near Flatland can generate weak mountain waves as a limiting case. Over horizontal scales of kilometers, the slopes of Yankee Ridge are only about 1°, although with a 10 m s^{-1} surface wind and assuming mountain wave streamlines with similar tilts as those of the land surface, this gives $W \sim 0.2$ m s^{-1}. The correlation between variance of W and long-term mean $\overline{W}$ shown by Nastrom and VanZandt (1994, Fig. 7) is also not inconsistent with mountain waves. Patterns of convective activity near the Flatland site (Angevine 1997), with enhanced convection above the nearby ''heat island'' of Champaign–Urbana city, may also have some effect. Huff et al. (1975) show that nearby small hills of 120 m in southern Illinois do affect the atmosphere, causing enhanced rainfall. Even if a flatter site is found, the long-term effect on $\overline{W}$ of slight horizontal variations in convective activity, ''thermals,'' the updrafts disturbing the airflow in a similar way to hills (e.g., Kuettner et al. 1987) is uncertain. Convective launching of waves may also occur commonly above mountains (Worthington 2000, manuscript submitted to *Quart. J. Roy. Meteor. Soc.*). Maybe the only genuinely flat radar location would be a small, very low island, in midlatitudes and not the Tropics in order to reduce convective effects, and surrounded by hundreds of kilometers of ocean (perhaps like Rockall Island—20 m high, 90 m circumference, in the North Atlantic, hundreds of km from land), leaving only the problems caused by models 3 and 4 to be resolved.

Evidence for model 3, in terms of a relation between $\overline{W}$ and the correlation of W and vertical echo power (r_{wp}), measured at 75-m vertical resolution using the Sounding System (SOUSY) radar, is shown by Nastrom et al. (1998). They report that the correlation coefficients between W and r_{wp}, $+0.1$ to $+0.2$, although very small, could be statistically significant. However, W and r_{wp} are two from a total of tens or hundreds of possible atmospheric and radar-measured parameters, and each parameter from the total will be correlated in the long term, at least slightly, with many others. For instance, patchy regions of air with finescale horizontal layering, capable of giving aspect-sensitive VHF backscatter, that become slightly tilted as they are advected through steady mountain waves above a radar (Worthington 1999a), would perturb both W and echo power. Figure 4 of Nastrom et al. (1998) shows that the entire scatterplot of W against r_{wp} appears to be shifted to downward W. For instance, when the perturbations of W and stability are uncorrelated ($r_{wp} = 0$), the predicted $\overline{W}$ bias should be zero—yet it remains approximately 5 cm s^{-1} downward. The lower right-hand side ($r_{wp} > 0$) of their Fig. 4, where the correlation of W and r_{wp} is now of the wrong sign for model 3, also shows a downward $\overline{W}$ only slightly less pronounced than for $r_{wp} < 0$. The cause of downward $\overline{W}$ in their Fig. 4 appears almost independent of the relative sign of W and r_{wp}. A possible explanation for downward $\overline{W}$ at the mountainous SOUSY location that is not dependent on a correlation of W and r_{wp}, is mountain waves, model 5.

e. Phase relation between mountain wave clouds and the mountains below

The W in individual mountain wave events can reach ± 3 m s^{-1} or more, which is 100 times greater than the small long-term mean $\overline{W}$ in Fig. 5. If $\overline{W}$ above Aberystwyth is caused by a residual mountain wave component (model 5), then large-amplitude variations have to be almost averaged away over long timescales, presumably both by the ''dilution'' of the $\overline{W}$ profile by calm days with no mountain waves, and by phase variations of the mountain waves above the radar. For instance, the magnitude of $\overline{W}$ in Fig. 5 is about 10% of W in Fig. 7, which is from a typical mountain wave event; however, mountain waves are observed more than 10% of the time at Aberystwyth (Prichard et al. 1995). Therefore, phase variations of W above the radar, and not just the inclusion of calm days, must be contributing to the reduction of magnitude of long-term $\overline{W}$.

For sharp mountain ridges, a mountain wave pattern can remain closely phase-locked to the mountain, as shown by persistent wave clouds such as the Helm Bar cloud of northern England (Manley 1945), or near the Front Range of the Rocky Mountains in Colorado. Over timescales of hours, this has also been reported above the Welsh mountains (George 1959). Long-term measurements of mountain wave launching height (Worthington 1999b) suggest, however, that the waves are only quite weakly coupled or phase-locked to detailed

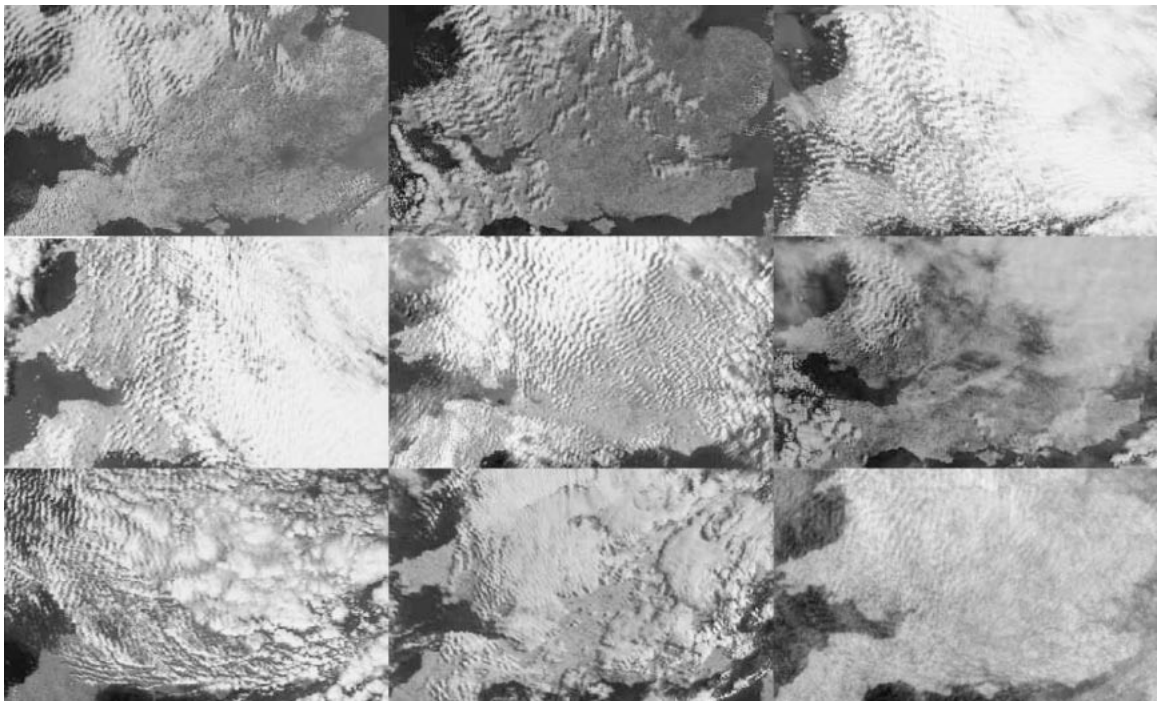

FIG. 11. Eight individual NOAA satellite images of Wales and south England, showing mountain wave clouds above Wales, and (lower right) the average of these images. North is at the top of the images, Wales is in the northwest, and the land height is shown in Fig. 10 (Aberystwyth) and by Worthington (1999b, Fig. 1). In the averaged image, the coastline remains sharp, so the relative positioning of individual images is accurate; however, the average wave cloud pattern becomes fainter, as if the wave cloud positions are not tightly fixed relative to the mountains. The faint cloud bands that remain do not match up with mountain ridges; some are seen over the sea. When more images are averaged together, the cloud bands disappear as shown in Fig. 12.

FIG. 12. Average of 50 individual NOAA satellite images of mountain wave clouds, similar to those in Fig. 11, during years 1996–99. Regions of bare land surface and nonorographic cloud are deleted from individual images, leaving only the sea, coastline, and areas of wave cloud, in similar quantities, which are averaged together to give the above image. The coastline, including features of horizontal scale only a few kilometers, remains sharp; however, the wave-cloud patterns have almost disappeared. Therefore, it appears that the positions of mountain wave cloud bands are often not tightly fixed, relative to the hills and valleys below.

terrain features; the boundary-layer wind structure is more important for the alignment of the wave pattern. Brown (1983, Fig. 3, flight H389) presents a case study showing little phase relation between peaks and troughs of mountain waves and the Welsh hills and valleys below. Similar results near south Wales are shown by Nicholls (1973). Even the persistent mountain wave cloud described by Manley (1945) showed horizontal variations in position of many kilometers, relative to the mountain.

This lack of close phase locking between mountain waves and the mountains can be demonstrated using satellite images (Fig. 11). Eight images show clear mountain wave clouds above Wales. In the upper six images the wave clouds all have similar NE–SW alignments, in the last two images the alignments are nearer N–S and NW–SE, but in all, the wave-cloud patterns are quite regular. A simple numerical average of the eight images is shown in Fig. 11, lower right. The wave clouds in the average image are fainter than in the individual images, yet detailed features of the coastline, of similar horizontal scale as the wave clouds, remain sharp. This shows that image positioning errors are not blurring away the average wave-cloud pattern. Also, in an average of 50 satellite images with similar mountain wave clouds (Fig. 12), and with the regions of nonorographic cloud and bare land surface digitally masked

off, only the coastline in the average image can be seen. The positions of wave clouds are sufficiently random that they average almost to zero. Nance and Durran (1997) show how lee waves, downwind of a mountain, can move upwind and downwind, changing their phase relative to the ground; Fig. 12 shows that this can also occur for waves directly above the mountains. Therefore, the steady phase-locked situation shown in Fig. 3 is valid only in a long-term statistical sense, although, for the hydrostatic mountain waves in section 3b, this may be enough to explain the small nonzero observed $\overline{W}$ profile in Fig. 5.

f. Review of possibly unexplained measurements

Chau and Balsley (1998) find that $\overline{W}$ profiles using the Jicamarca radar are affected by the choice of radar beamwidth; $\overline{W}$ profiles from a broad beam show downward motion in the troposphere and upward motion in the stratosphere, but this disappears when an extremely narrow beam is used instead. This is consistent with a dependence of $\overline{W}$ on beamwidth shown by Muschinski (1996) for model 4; however, the site is far from jet streams, and the vertical shear of horizontal wind (Chau and Balsley 1998, their Fig. 5) does not show a simple reversal of sign between troposphere and stratosphere. Disagreements are also seen using a wide range of spatial interferometry methods to measure $\overline{W}$. These differences remain unexplained at present.

McAfee et al. (1994, 1995) show $\overline{W}$ measured using collocated UHF and VHF radars at Platteville, Colorado. Compared to VHF radar, UHF echoes are less affected by aspect sensitivity, and more sensitive to precipitation. The site is on relatively low ground (Fig. 10) about 40 km east of the Rocky Mountains—probably not far enough, in comparison to typical mountain wave horizontal wavelengths, for the phase of mountain lee waves above these radars to be random. Both the VHF and UHF radars measure downward $\overline{W}$ over a large height range, 5–18 km, which the authors suggest may be orographic. Possibly $\overline{W}$ shows large-scale descent of prevailing westerly winds, given the great decrease in land height, by a few thousand meters, from the Rocky Mountains to the Great Plains. VHF vertical-beam data from Platteville were examined for the present study (August 1994–May 1995, not shown) and $\overline{W}$ was very similar to the results of McAfee et al. (1995). The radar was operated with only three beams, so calculation of $\overline{W}$ from symmetric beam pairs was not possible.

At the SOUSY radar, published $\overline{W}$ profiles (Yoe and Rüster 1992, their Figs. 1–3) may seem to have insufficient height gap between the lowest radar range gate and the ground, for $\overline{W}$ to reverse sign and become slightly positive as in Fig. 3. However, Fig. 10 shows this radar is sited very close to the base of a mountain, on the upwind side for prevailing westerly winds. In Fig. 3 this correponds to radar position being shifted to the right, so that the region of lower-tropospheric upward $\overline{W}$ is less high, as observed. [However, although the $\overline{W}$ profiles shown by Yoe and Rüster (1992) and Yoe et al. (1994) are similar to measurements at Aberystwyth in Fig. 6 and 7, attempts to repeat the aspect sensitivity observations of Yoe et al. (1994) using Aberystwyth data have so far been unsuccessful.]

Larsen and Röttger (1991) describe upward tropospheric $\overline{W}$, measured by the vertical beam of the SOUSY radar, which persisted for most of a day or two, and was not believed to be real. When correction was made for the tilt angles of the aspect-sensitive scatterers measured by spatial interferometry, the upward $\overline{W}$ disappeared. Another possibility is that the temporary upward $\overline{W}$ was mostly real and caused by a mountain wave, and it disappeared because the airflow and the scatterers were tilted by similar angles, that is, Larsen and Röttger (1991) assumed the situation was as in Fig. 2a, whereas it was closer to Fig. 2b. Whether the remaining $\overline{W}$ after the correction was made is an accurate synoptic-scale value remains uncertain, as there were system configuration problems (May 1993).

Balsley and Carter (1989) find upward $\overline{W}$ in the troposphere, using the Pohnpei radar. However the site is at the base of a high, isolated mountain, expected to give a ''ship wave'' type pattern of mountain waves. It is not certain what long-term phase of the waves is seen, and there is no inconsistency with model 5.

In Figs. 5 and 7 of the present study, zonal wind measured by VHF radar becomes several meters per second greater than that measured by radiosondes, above ~15 km. The radar and sonde measurements in Fig. 5 disagree slightly because the times being averaged are not identical, but VHF radar usually underreads horizontal wind speeds because of aspect sensitivity [e.g., Thomas et al. (1997) for the height range 4–14 km at Aberystwyth], so the increased long-term difference above 15 km needs to be understood. There are also interesting time variations of horizontal wind speed above 12 km in Fig. 6e. Detailed comparison of Fig. 6e and Figs. 6a–c suggests that positive (negative) perturbations of horizontal wind speed match downward (upward) W. This phase relation between the horizontal and vertical wind perturbations is of the correct sign for an untrapped mountain wave. Above about 15 km, downward W is more common than upward, for exactly the same reason that causes downward midtropospheric $\overline{W}$; the Aberystwyth radar location is on low ground (model 5). Therefore, mountain wave perturbations could also bias horizontal wind measurements. The problem may be more noticeable in the stratosphere because the increased stability increases the ratio of horizontal to vertical wind perturbations in the mountain wave (e.g., Hines 1989). Radiosonde horizontal-wind measurements would be less affected in the long term [although individual sondes would still be affected (Pitts and Lyons 1988)], because the phase relation between sonde position and the mountain wave pattern is relatively random; the horizontal tracks of released radiosondes

are quite variable, being the cumulative effect of the height-varying horizontal wind vector, and by the height of 15 km the radiosonde may be downwind of the Welsh mountains and out of the mountain waves anyway. Only radars, having fixed location relative to the mountains and mountain waves, may be affected long term. However, this problem caused by mountain waves in Figs. 5–7 does not undermine model 5, but is further evidence in support of it.

In addition, it might be interesting to study the synoptic-scale tilts associated with the jet stream itself, as well as the KHI within it, since the movement of ''layers'' detected by frequency domain interferometry (e.g., Muschinski et al. 1999) could actually represent the movement and tilting of layers with much smaller vertical scales (Luce et al. 1999), capable of causing VHF-aspect-sensitivity biases similar to model 4 (Muschinski 1996). The long-term result of the location and motion patterns of the jet stream relative to wind-profiling radars, on timescales of years, is unclear. Similarly, the preferred phase of inertia-gravity waves relative to the jet maximum, having a small but real W component, might also have a slight effect.

4. Conclusions

A new mountain wave model for mean vertical wind ($\overline{W}$) measured by wind-profiling radars has been described and tested. It is consistent with published results from many radars, mostly unexplained, such as:

1) The agreement often found between $\overline{W}$ profiles measured by different radar beam combinations, for example, between vertical beam and symmetric beam pairs 15° off-vertical (Nastrom and VanZandt 1994, Fig. 6), between UHF and VHF radars (McAfee et al. 1994, 1995), and using vertical-beam and ''velocity-azimuth display''-type methods (Yoe and Rüster 1992; Yoe et al. 1994). The effect of tilted aspect-sensitive scatterers (model 4) should usually be less for beams at large off-zenith angles, yet $\overline{W}$ from symmetric pairs of these beams often agrees with vertical-beam measurements, as if the $\overline{W}$ bias is not closely related to aspect sensitivity. However, for a real, residual mountain wave component (model 5) measurements of $\overline{W}$ from symmetric beam pairs at any off-zenith angle should be similar, if the horizontal beam separation is small relative to λ_x of the waves, and aspect sensitivity is of relatively minor importance.
2) The magnitude of W variations, approaching ± 1 m s^{-1}, found by Yoe and Rüster (1992) is extremely large for synoptic-scale vertical winds, especially in the stratosphere, but typical for mountain waves.
3) Extra reversals of the sign of $\overline{W}$, upward below 3 km and downward above 16 km as shown in Fig. 1c (Worthington 1999a, Fig. 10), would be expected for mountain waves (model 5) but not the other models 1–4.

None of models 1–4 discussed in section 1 is disproved, and the actual cause of $\overline{W}$ in any particular midtropospheric radar measurement is possibly a combination of some or all five models, with the relative contribution from each being difficult to measure. However, only the new mountain wave model 5 explains case studies such as Fig. 7, and long-term average profiles as in Figs. 1c, 5.

Finally, a prediction from the mountain wave model 5 discussed in this paper is as follows: if a VHF wind-profiling radar could be built on high ground near the center of a mountain range (e.g., Hafren Forest in the mountains near Aberystwyth), and W measurements could be taken for several years, the long-term $\overline{W}$ profile would be the reverse of Fig. 1c, mostly upward $\overline{W}$ below 10 km and downward above 10 km, provided that the mountain wave effect on $\overline{W}$ (model 5) dominates the other models 1–4. Except for the difficulty of building a radar on a suitable high-altitude site, this may be a simpler and more robust test of the topographic effect on $\overline{W}$ than finding a very flat site.

Acknowledgments. The Piura radar is part of the University of Colorado/NOAA Pacific profiler network, and is partially funded by the National Science Foundation under ATM-96/46/3. Data from final (FNL) runs of the NCEP GDAS model were provided by the NOAA Air Resources Laboratory. The Aberystwyth MST radar is a U.K. national facility of the Natural Environment Research Council (NERC). Radiosonde data are by the U.K. Meteorological Office. U.K. radar and radiosonde data are supplied by the NERC British Atmospheric Data Centre, and NOAA satellite images by the University of Strasbourg, France. Topographic data from the Global Land One-kilometer Base Elevation (GLOBE) database are supplied by the NOAA National Geophysical Data Center. Programs to extract Piura radar data were provided by J. L. Chau of Jicamarca Radio Observatory, Perú, and Australian data in Table 1 by D. A. Holdsworth of ATRAD.

REFERENCES

Angevine, W. M., 1997: Errors in mean vertical velocities measured by boundary layer wind profilers. *J. Atmos. Oceanic Technol.*, **14,** 565–569.

Asimakopoulos, D. N., D. G. Deligiorgi, and D. P. Lalas, 1980: Acoustic sounder observations of the atmospheric boundary layer from the top of a steep mountain. *J. Appl. Meteor.*, **19,** 109–112.

Balsley, B. B., and D. A. Carter, 1989: Mountain waves in the tropical Pacific atmosphere: A comparison of vertical wind fluctuations over Pohnpei and Christmas Island using VHF wind profilers. *J. Atmos. Sci.*, **46,** 2698–2715.

——, W. L. Ecklund, D. A. Carter, A. C. Riddle, and K. S. Gage, 1988: Average vertical motions in the tropical atmosphere observed by a radar wind profiler on Pohnpei (7°N lat, 157°E long). *J. Atmos. Sci.*, **45,** 396–405.

Bishop, B. B., 1968: Lee waves over the Welsh mountains. *Sailplane Gliding,* **19,** 94–95.

Bougeault, P., B. Benech, P. Bessemoulin, B. Carissimo, A. Jansa Clar, J. Pelon, M. Petitdidier, and E. Richard, 1997: PYREX: A summary of findings. *Bull. Amer. Meteor. Soc.,* **78,** 637–650.

Bradbury, T. A. M., 1965: Wave clouds over Berkshire. *Weather,* **20,** 16–17.

Brown, P. R. A., 1983: Aircraft measurements of mountain waves and their associated momentum flux over the British Isles. *Quart. J. Roy. Meteor. Soc.,* **109,** 849–865.

Caccia, J.-L., B. Benech, and V. Klaus, 1997a: Space–time description of nonstationary trapped lee waves using ST radars, aircraft, and constant volume balloons during the PYREX experiment. *J. Atmos. Sci.,* **54,** 1821–1833.

——, M. Crochet, and K. Saada, 1997b: ST radar evaluation of the standard deviation of the air vertical velocity perturbed by the local orography. *J. Atmos. Solar-Terr. Phys.,* **59,** 1127–1131.

Chau, J. L., and B. B. Balsley, 1998: A statistical comparison of VHF techniques to study clear-air vertical velocities in the lower atmosphere using the Jicamarca radar. *Radio Sci.,* **33,** 1565–1583.

Faust, H., 1962: The dynamical signifance of null layers; layers of zero or vanishing vertical motion. *Weather,* **17,** 285–295.

Fukao, S., M. F. Larsen, M. D. Yamanaka, H. Furukawa, T. Tsuda, and S. Kato, 1991: Observations of a reversal in long-term average vertical velocities near the jet stream wind maximum. *Mon. Wea. Rev.,* **119,** 1479–1489.

Gage, K. S., 1986: Implications of tilting of stable layers on atmospheric measurements by clear-air Doppler radars. Preprints, *23d Conf. on Radar Meteorology,* Snowmass, CO, Amer. Meteor. Soc., 30–33.

——, J. R. McAfee, D. A. Carter, W. L. Ecklund, A. C. Riddle, G. C. Reid, and B. B. Balsley, 1991: Long-term mean vertical motion over the tropical Pacific: Wind-profiling Doppler radar measurements. *Science,* **254,** 1771–1773.

——, ——, and G. C. Reid, 1992: Diurnal variation in vertical motion over the central equatorial Pacific from VHF wind-profiling Doppler radar observations at Christmas Island (2°N, 157°W). *Geophys. Res. Lett.,* **19,** 1827–1830.

Gardiner, B. A., and M. K. Hill, 1986: Acoustic sounder observations from an elevated location. *Bound.-Layer Meteor.,* **36,** 307–316.

Gedzelman, S. D., 1977: Mountain wave weather in New York City. *Weatherwise,* **30,** 202–206.

George, D. J., 1959: A persistent wave cloud over north Breconshire, 13 April 1958. *Weather,* **14,** 233–236.

Gill, A. E., 1982: *Atmosphere–Ocean Dynamics.* Academic Press, 662 pp.

Green, J. L., and K. S. Gage, 1980: Observations of stable layers in the troposphere and stratosphere using VHF radar. *Radio Sci.,* **15,** 395–405.

Hensman, G. W. J., 1971: Wave in a fog top. *Weather,* **26,** 58–60.

Hines, C. O., 1989: Tropopausal mountain waves over Arecibo: A case study. *J. Atmos. Sci.,* **46,** 476–488.

Hoppe, U.-P., and D. C. Fritts, 1995: On the downward bias in vertical velocity measurements by VHF radars. *Geophys. Res. Lett.,* **22,** 619–622.

Huaman, M. M., and B. B. Balsley, 1996: Long-term average vertical motions observed by VHF wind profilers: The effect of slight antenna-pointing inaccuracies. *J. Atmos. Oceanic Technol.,* **13,** 560–569.

Huff, F. A., S. A. Changnon, and D. M. A. Jones, 1975: Precipitation increases in the low hills of southern Illinois. Part 1: Climatic and network studies. *Mon. Wea. Rev.,* **103,** 823–329.

Kuettner, J. P., P. A. Hildebrand, and T. L. Clark, 1987: Convection waves: Observations of gravity wave systems over convectively active boundary layers. *Quart. J. Roy. Meteor. Soc.,* **113,** 445–467.

Larsen, M. F., and J. Röttger, 1991: VHF radar measurements of in-beam incidence angles and associated vertical-beam radial velocity corrections. *J. Atmos. Oceanic Technol.,* **8,** 477–490.

——, S. Fukao, O. Aruga, M. D. Yamanaka, T. Tsuda, and S. Kato, 1991: A comparison of VHF radar vertical-velocity measurements by a direct vertical-beam method and by a VAD technique. *J. Atmos. Oceanic Technol.,* **8,** 766–776.

Lee, G. H., and O. W. Neumark, 1952: A standing wave at Dunstable. *Meteor. Mag.,* **81,** 307–310.

Lenschow, D. H., S. F. Zhang, and B. B. Stankov, 1988: The stably stratified boundary layer over the Great Plains. *Bound.-Layer Meteor.,* **42,** 123–135.

Liziola, L. E., and B. B. Balsley, 1998: Studies of quasi horizontally propagating gravity waves in the troposphere using the Piura ST wind profiler. *J. Geophys. Res.,* **103,** 8641–8650.

Luce, H., M. Crochet, C. Hanuise, M. Yamamoto, and S. Fukao, 1999: On the interpretation of the layered structures detected by mesosphere–stratosphere–troposphere radars in dual frequency domain interferometry mode. *Radio Sci.,* **34,** 1077–1083.

Manley, G., 1945: The Helm wind of Crossfell, 1937–1939. *Quart. J. Roy. Meteor. Soc.,* **71,** 197–220

May, P. T., 1993: Comments on ''VHF radar measurements of in-beam incidence angles and associated vertical-beam radial velocity corrections.'' *J. Atmos. Oceanic Technol.,* **10,** 432–434.

McAfee, J. R., B. B. Balsley, and K. S. Gage, 1989: Momentum flux measurements over mountains: Problems associated with the symmetrical two-beam radar technique. *J. Atmos. Oceanic Technol.,* **6,** 500–508.

——, K. S. Gage, and R. G. Strauch, 1994: Examples of vertical velocity comparison from collocated VHF and UHF profilers. *Radio Sci.,* **29,** 879–880.

——, ——, and ——, 1995: Vertical velocities at Platteville, Colorado: An intercomparison of simultaneous measurements by the VHF and UHF profilers. *Radio Sci.,* **34,** 1027–1042.

Muschinski, A., 1996: Possible effect of Kelvin–Helmholtz instability on VHF radar observations of the mean vertical wind. *J. Appl. Meteor.,* **35,** 2210–2217.

——, P. B. Chilson, S. Kern, J. Nielinger, G. Schmidt, and T. Prenosil, 1999: First frequency-domain interferometry observations of large-scale vertical motion in the atmosphere. *J. Atmos. Sci.,* **56,** 1248–1258.

Nance, L. B., and D. R. Durran, 1997: A modeling study of nonstationary trapped mountain lee waves. Part I: Mean-flow variability. *J. Atmos. Sci.,* **54,** 2275–2291.

Nastrom, G. D., 1984: Detection of synoptic-scale vertical velocities using an MST radar. *Geophys. Res. Lett.,* **11,** 57–60.

——, and T. E. VanZandt, 1994: Mean vertical motions seen by radar wind profilers. *J. Appl. Meteor.,* **33,** 984–995.

——, and F. D. Eaton, 1995: Variations of winds and turbulence seen by the 50-MHz radar at White Sands Missile Range, New Mexico. *J. Appl. Meteor.,* **34,** 2135–2148.

——, and T. E. VanZandt, 1996: Biases due to gravity waves in wind profiler measurements of winds. *J. Appl. Meteor.,* **35,** 243–257.

——, W. L. Ecklund, and K. S. Gage, 1985: Direct measurement of large-scale vertical velocities using clear-air Doppler radars. *Mon. Wea. Rev.,* **113,** 708–718.

——, M. R. Peterson, J. L. Green, K. S. Gage, and T. E. VanZandt, 1990: Sources of gravity wave activity seen in the vertical velocities observed by the Flatland VHF radar. *J. Appl. Meteor.,* **29,** 783–1792.

——, R. Rüster, and G. Schmidt, 1998: The coupling of vertical velocity and signal power observed with the SOUSY VHF radar. *J. Appl. Meteor.,* **37,** 114–119.

Nicholls, J. M., 1973: Aircraft measurements of disturbed airflow over mountains. *Weather,* **28,** 141–152.

Palmer, R. D., M. F. Larsen, R. F. Woodman, S. Fukao, M. Yamamoto, T. Tsuda, and S. Kato, 1991: VHF radar interferometry measurements of vertical velocity and the effect of tilted refractivity surfaces on standard Doppler measurements *Radio Sci.,* **26,** 417–427.

Pitts, R. O., and T. J. Lyons, 1988: The influence of topography on Perth radiosonde observations. *Aust. Meteor. Mag.,* **36,** 17–23.

Prichard, I. T., L. Thomas, and R. M. Worthington, 1995: The char-

acteristics of mountain waves observed by radar near the west coast of Wales. *Ann. Geophys.,* **13,** 757–767.

Rao, D. N., S. Thulasiraman, S. V. B. Rao, T. N. Rao, P. Kishore, M. V. Ratnam, and K. K. Reddy, 2000: VHF radar observations of tropical easterly jet stream over Gadanki. *Adv. Space Res.,* **26,** 943–946.

Röttger, J., C. H. Liu, J. K. Chen, A. J. Chen, C. J. Pan, and I. J. Fu, 1990: Spatial interferometer measurements with the Chung-Li VHF radar. *Radio Sci.,* **25,** 503–515.

Slater, K., and Coauthors, 1992: (Overview of the MST radar system at Aberystwyth. *Proc. Fifth Workshop on Technical and Scientific Aspects of MST radar,* Aberystwyth, Wales, Scientific Committee on Solar Terrestrial Physics, 479–482.

Takayabu, I., M. D. Yamanaka, and S. Fukao, 2000: A mechanism for the reversal of long-term average vertical velocities around East Asia during the cold season. *J. Meteor. Soc. Japan,* **78,** 13–23.

Thomas, L., I. Astin, and R. M. Worthington, 1997: A statistical study of underestimates of wind speeds by VHF radar. *Ann. Geophys.,* **15,** 805–812.

United States Geological Survey, 1957a: Mahomet quadrangle Illinois, 1:62500 scale topographic map. United States Geological Survey.

——, 1957b: Urbana quadrangle, Illinois-Champaign Co., 1:62500 scale topographic map. United States Geological Survey.

VanBaelen, J. S., A. D. Richmond, T. Tsuda, S. K. Avery, S. Kato, S. Fukao, and M. Yamamoto, 1991: Radar interferometry technique and anisotropy of the echo power distribution: First results. *Radio Sci.,* **26,** 1315–1326.

Van den Dool, H. M., 1990: Time-mean precipitation and vertical motion patterns over the United States. *Tellus,* **42A,** 51–64.

VanValin, C. C., R. F. Pueschel, E. W. Barrett, and G. M. Williams, 1982: Field observations of stratified atmospheric flow above an obstacle. *Bound.-Layer Meteor.,* **24,** 331–343.

Wallington, C. E., 1961: Airflow over broad mountain ranges—A study of five flights across the Welsh mountains. *Meteor. Mag.,* **90,** 213–222.

Warnock, J. M., T. E. VanZandt, W. L. Clark, S. J. Franke, H. S. Kim, G. D. Nastrom, and P. E. Johnston, 1994: Measurements of synoptic-scale vertical velocities by two nearby VHF Doppler radars in very flat terrain. *J. Atmos. Oceanic Technol.,* **11,** 5–13.

Worthington, R. M., 1998: Tropopausal turbulence caused by the breaking of mountain waves. *J. Atmos. Solar-Terr. Phys.,* **60,** 1543–1547.

——, 1999a: Calculating the azimuth of mountain waves, using the effect of tilted finescale stable layers on VHF radar echoes. *Ann. Geophys.,* **17,** 257–272.

——, 1999b: Alignment of mountain wave patterns above Wales: A VHF radar study during 1990–1998. *J. Geophys. Res.,* **104,** 9199–9212.

——, and L. Thomas, 1996a: Radar measurements of critical-layer absorption in mountain waves. *Quart. J. Roy. Meteor. Soc.,* **122,** 1263–1282.

——, and ——, 1996b: The measurement of gravity wave momentum flux in the lower atmosphere using VHF radar. *Radio Sci.,* **31,** 1501–1517.

——, and ——, 1997a: Long-period unstable gravity-waves and associated VHF radar echoes. *Ann. Geophys.,* **15,** 813–822.

——, and ——, 1997b: Impact of the tropopause on upward propagation of mountain waves. *Geophys. Res. Lett.,* **24,** 1071–1074.

——, and ——, 1998: The frequency spectrum of mountain waves. *Quart. J. Roy. Meteor. Soc.,* **124,** 687–703.

Yoe, J. G., and R. Rüster, 1992: VHF Doppler radar observations of vertical velocities in the vicinity of the jet stream. *Mon. Wea. Rev.,* **120,** 2378–2382.

——, P. Czechowsky, R. Rüster, and G. Schmidt, 1994: Spatial variability of the aspect sensitivity of VHF radar echoes in the troposphere and lower stratosphere during jet stream passages. *Ann. Geophys.,* **12,** 733–745.